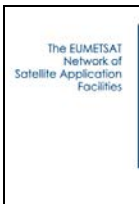# The Zeeman effect implementation for SSMIS in ARTS v. RTTOV

Richard Larsson

Luleå University of Technology, Division of Space Technology, Rymdcampus 1, SE-98192 Kiruna, Sweden

The Zeeman effect implementation for SSMIS in ARTS v. RTTOV

Richard Larsson

Luleå University of Technology, Division of Space Technology, Rymdcampus 1, SE-98192 Kiruna, Sweden

This documentation was developed within the context of the EUMETSAT Satellite Application Facility on Numerical Weather Prediction (NWP SAF), under the Cooperation Agreement dated 29 June 2011, between EUMETSAT and the Met Office, UK, by one or more partners within the NWP SAF. The partners in the NWP SAF are the Met Office, ECMWF, KNMI and Météo France.

Change record			
Version	Date	Author / changed by	Remarks
1.0	16/6/14	R. Larsson	

The Zeeman effect implementation for SSMIS in ARTS v. RTTOV

Richard Larsson

June 16, 2014

Abstract

This document is the report specified by NWP VS13 P02 as part of my visit to Met Office in early spring of 2014. On site, we changed the details of the contract to work only with SSMIS, as this instrument is more strongly affected by the Zeeman Effect so the comparison is more urgent. The main conclusion is that ARTS and RTTOV agree within error of the instrument itself, but that there are systematic biases between the two models. Some, maybe all, of these systematic biases are identified in this report. Some recommendations of improvements to RTTOV-11 are presented at the end of the report.

1 Introduction

The Atmospheric Radiative Transfer Simulator (ARTS) is a full 3D radiative transfer simulation suite for microwave radiation in any planetary atmosphere operating in Stokes formalism. ARTS calculates the spectral intensity line-by-line during every run for the input atmospheric scenario.

The Radiative Transfer model for Television Infrared Observation Satellites Operational Vertical Sounder (RTTOV) is a downward-looking fast radiative transfer suite for multiple Earth-orbiting satellites. RTTOV achieves its speed by using pre-calculated coefficients to predict the optical depths used in the radiative transfer integration.

The Zeeman (1897) effect changes spectral features as a function of the magnetic field. This is done by splitting what is otherwise one line into several lines, a fine structure, that are polarized as a function of the orientation of the magnetic field. The Zeeman effect is important for describing radiation from upper atmospheric O_2, which is measured by, e.g., the Advanced Microwave Sounder Unit A (AMSU-A) and the Special Sensor Microwave Imager/Sounder (SSMIS). This report will only focus on SSMIS. Assimilation of radiances including the Zeeman effect has turned out to be quite difficult. Kobayashi et al. (2009) used an old version of RTTOV to look at

assimilation. Still, their work shows that there is much missing in understanding and modeling the Zeeman effect for upper O_2 satellite measurements to concord with other measurements and restrain numerical weather prediction models.

The goal of this report is to identify similarities and dissimilarities between how ARTS and RTTOV computes the Zeeman effect on radiation transfer in Earth's atmosphere for SSMIS channels 19-22. ARTS calculate the Zeeman effect by splitting each affected input line in all layers and then solving the polarized radiative transfer in Stokes formalism for each layer for each line. The magnetic field can be input either as a constant or as a full field. RTTOV pre-calculate its coefficients for the Zeeman effect in select atmospheric scenarios in coherency formalism using either the Amsutran code or the work by Han et al. (2007). The magnetic field is input with a constant strength and angle throughout the radiation path. The polarization of the radiation is selected based on the channel of interest and will be built into the coefficients.

2   Theory

ARTS uses Stokes formalism and tracks the radiation as it passes through the atmosphere. This tracking is done by incrementally solving the vector radiative transfer equation (see, e.g., del Toro Iniesta, 2004)

$$\frac{d\vec{I}}{d\vec{r}} = -\mathbf{K} \left[\vec{I} - \vec{B}(T) \right]$$ (1)

for homogeneous atmospheric layers. In the above equation, $\vec{I}$ is the Stokes vector, $\vec{r}$ is the position vector, $\mathbf{K}$ is the propagation matrix, and $\vec{B}$ is the Planck function in Stokes vector format for temperature T. The Stokes vector is in this work defined as

$$\vec{I} = \begin{bmatrix} I \\ Q \\ U \\ V \end{bmatrix},$$ (2)

where I is the total intensity of perpendicular polarizations, Q is the difference between vertical and horizontal linear polarization, U is the difference between off-axis linear polarizations ($\pm 45°$), and V is the level of circular phase delay, with positive values meaning left circular polarization dominant. Examples: a sensor measuring left circular polarization sees $I/2 + V/2$, and a sensor measuring horizontal polarization sees $I/2 - Q/2$. For details on the input and how each part of Equation 1 is calculated for the Zeeman effect, please see the work by Larsson et al. (2014) and sources therein.

2

The solution to the Stokes vector radiative transfer equation for finite homogeneous layers is written

$$\vec{I}_{\text{out}} = \exp\left(-\mathbf{K}_i r_i\right)\vec{I}_{\text{in}} + \left[\mathbf{1} - \exp\left(-\mathbf{K}_i r_i\right)\right]\vec{B}(T_i), \tag{3}$$

where the index i signifies that the variable is a function of the layer, r_i being the distance the radiation travels in the layer, and $\mathbf{1}$ is the 4×4 identity matrix. The Stokes vectors $\vec{I}_{\text{in}}$ and $\vec{I}_{\text{out}}$ respectively represent polarized radiation intensity going into the layer that will travel toward the sensor, and polarized radiation intensity going out of the layer that will travel toward the sensor.

ARTS is monochromatic. After the final layer, each monochromatic simulation within the frequency bin that the channel measures are added together and averaged for a final output. Sufficiently many monochromatic simulations must be done so that the line shape is properly resolved. We decided that this meant around 5 kHz resolution for SSMIS and its higher altitude channels (yielding about 20 simulation points per Doppler line shape, of which there is one per Zeeman split line).

ARTS calculates the path the radiation will take from a defined background source to the sensor. In this comparison, the background source is always the planetary surface. Each layer property is then calculated as the average of the two surrounding levels. Using half integer levels to represent the input value of a level, ARTS defines the integer layer properties as

$$r_i = \frac{1}{2}\left|\left(\vec{r}_{i-1/2} + \vec{r}_{i+1/2}\right)\right|, \tag{4}$$

$$\mathbf{K}_i = \frac{1}{2}\left(\mathbf{K}_{i-1/2} + \mathbf{K}_{i+1/2}\right), \text{ and} \tag{5}$$

$$B(T_i) = \frac{1}{2}\left[\vec{B}\left(T_{i-1/2}\right) + \vec{B}\left(T_{i+1/2}\right)\right]. \tag{6}$$

RTTOV does not compute the radiative transfer equation directly. Instead, it utilizes a solution of the scalar unpolarized radiative transfer equation by integrating the transmissions along the path. Thus, the output from RTTOV is calculated as

$$I = \int B(T)d\tau\left(\vec{r}\right), \tag{7}$$

where B is the scalar Planck function and τ is the transmission to the sensor from position $\vec{r}$ on the path. This integral is itself calculated as

$$I = \sum_i^N B(T_i)\Delta\tau(T_i, \cdots), \tag{8}$$

where $\Delta\tau$ is the transmission that the sensor receives from the layer of temperature T_i and the triple dots means that the the effective transmission depends on many more parameters. RTTOV assumes polychromatic

transmission for the channel, and that the Planck function is calculated for the central frequency of the sensor channel for microwave radiation. The transmission $\Delta\tau(T_i, \cdots)$ is constructed to work for polychromatic transfer. RTTOV must be trained to have a matching set of predictors and coefficients that will calculate $\Delta\tau$ for a simulation. In all results of this work utilizing RTTOV directly, the coefficients have been generated by the work of Han et al. (2007). *Rayer* (personal communication) has generated new coefficients with Amsutran that produce mostly similar results as the coefficients by Han et al. (2007). I did not conduct any extensive testing on these new coefficients, so I will not include these in this report.

RTTOV calculates the path the radiation will take from the ground to the sensor, or from space to the ground to the sensor. Each layer is then defined as the average of the two surrounding levels. Using half integer levels to represent the input value of a level, RTTOV defines the integer layer properties as

$$r_i = \left| \left(\vec{r}_{i-1/2} + \vec{r}_{i+1/2} \right) / 2 \right|, \tag{9}$$

$$\Delta\tau(T_i, \cdots) = \Delta\tau \left(\left[T_{i-1/2} + T_{i+1/2} \right] / 2, \cdots \right), \text{ and} \tag{10}$$

$$B(T_i) = \vec{B} \left(\left[T_{i-1/2} + T_{i+1/2} \right] / 2 \right). \tag{11}$$

The last point is not strictly true because $B(T_i)$ is weighed by effective optical depth (the 'linear-in-tau' option) in RTTOV. Turning the weighting off did not produce noticeable differences in the comparisons, so I considered the above true in my work.

Amsutran is developed by *Rayer*, and is also able to calculate transmission changes due to the Zeeman effect using the work by Rosenkranz and Staelin (1988). Amsutran operates in the coherency formalism. In the coherency formalism, the radiative transfer equation is (see, e.g., Lenoir, 1967)

$$\frac{d\mathbf{L}}{dr} = - \left(\mathbf{G}\mathbf{L} + \mathbf{L}\mathbf{G}^\dagger \right) + B(T) \left(\mathbf{G} + \mathbf{G}^\dagger \right), \tag{12}$$

where $\mathbf{G}$ is the coherency propagation matrix, and $\mathbf{L}$ is the polarized radiation matrix. The radiative transfer equation through one layer is then

$$\mathbf{L}_{\text{out},i} = \mathbf{T}_i \mathbf{L}_{\text{in},i} \mathbf{T}_i^\dagger + \left(\mathbf{1} - \mathbf{T}_i \mathbf{T}_i^\dagger \right) B(T_i), \tag{13}$$

where I define $\mathbf{T}_i \equiv \exp(-\mathbf{G}_i r_i)$, and $\mathbf{T}_i^\dagger \equiv \exp(-\mathbf{G}_i^\dagger r_i)$. Amsutran calculates $\mathbf{T}_i$ for each layer and then describes the effective transmission from iteratively inserting $\mathbf{L}_{\text{out},i}$ as $\mathbf{L}_{\text{in},i+1}$ up until some level n so that $\mathbf{T}_n \mathbf{T}_n^\dagger = \mathbf{1}$. With full transmission, $\mathbf{L}_{\text{in},n}$ is then what reaches the sensor. In the way Amsutran defines the problem, we see that if only the thermal radiation of the ground and no reflection is considered, then the outgoing radiation of the first level is

$$\mathbf{L}_{\text{out},1} = \mathbf{T}_1 \mathbf{T}_1^\dagger B_0 + \left(\mathbf{1} - \mathbf{T}_1 \mathbf{T}_1^\dagger \right) B(T_1), \tag{14}$$

4

where B_0 is the thermal emission of the surface, the outgoing radiation of the second layer is

$$
\begin{aligned}
\mathbf{L}_{\text{out},2} = \mathbf{T}_2 \mathbf{T}_1 \mathbf{T}_1^\dagger \mathbf{T}_2^\dagger B_0 + \\
\left(\mathbf{T}_2 \mathbf{T}_2^\dagger - \mathbf{T}_2 \mathbf{T}_1 \mathbf{T}_1^\dagger \mathbf{T}_2^\dagger \right) B(T_1) + \\
\left(\mathbf{1} - \mathbf{T}_2 \mathbf{T}_2^\dagger \right) B(T_2),
\end{aligned}
\tag{15}
$$

the outgoing radiation of the third layer is

$$
\begin{aligned}
\mathbf{L}_{\text{out},3} = \mathbf{T}_3 \mathbf{T}_2 \mathbf{T}_1 \mathbf{T}_1^\dagger \mathbf{T}_2^\dagger \mathbf{T}_3^\dagger B_0 + \\
\left(\mathbf{T}_3 \mathbf{T}_2 \mathbf{T}_2^\dagger \mathbf{T}_3^\dagger - \mathbf{T}_3 \mathbf{T}_2 \mathbf{T}_1 \mathbf{T}_1^\dagger \mathbf{T}_2^\dagger \mathbf{T}_3^\dagger \right) B(T_1) + \\
\left(\mathbf{T}_3 \mathbf{T}_3^\dagger - \mathbf{T}_3 \mathbf{T}_2 \mathbf{T}_2^\dagger \mathbf{T}_3^\dagger \right) B(T_2) + \\
\left(\mathbf{1} - \mathbf{T}_3 \mathbf{T}_3^\dagger \right) B(T_3),
\end{aligned}
\tag{16}
$$

and the outgoing radiation of the last layer is

$$
\begin{aligned}
\mathbf{L}_{\text{out},n} = \mathbf{T}_n \cdots \mathbf{T}_1 \mathbf{T}_1^\dagger \cdots \mathbf{T}_n^\dagger B_0 + \\
\left(\mathbf{T}_n \cdots \mathbf{T}_2 \mathbf{T}_2^\dagger \cdots \mathbf{T}_n^\dagger - \mathbf{T}_n \cdots \mathbf{T}_1 \mathbf{T}_1^\dagger \cdots \mathbf{T}_n^\dagger \right) B(T_1) + \\
\left(\mathbf{T}_n \cdots \mathbf{T}_3 \mathbf{T}_3^\dagger \cdots \mathbf{T}_n^\dagger - \mathbf{T}_n \cdots \mathbf{T}_2 \mathbf{T}_2^\dagger \cdots \mathbf{T}_n^\dagger \right) B(T_2) + \\
\left(\mathbf{T}_n \cdots \mathbf{T}_4 \mathbf{T}_4^\dagger \cdots \mathbf{T}_n^\dagger - \mathbf{T}_n \cdots \mathbf{T}_3 \mathbf{T}_3^\dagger \cdots \mathbf{T}_n^\dagger \right) B(T_3) + \\
\cdots \quad \left(\mathbf{T}_n \cdots \mathbf{T}_{i+1} \mathbf{T}_{i+1}^\dagger \cdots \mathbf{T}_n^\dagger - \mathbf{T}_n \cdots \mathbf{T}_i \mathbf{T}_i^\dagger \cdots \mathbf{T}_n^\dagger \right) B(T_i) + \\
\cdots \quad \left(\mathbf{1} - \mathbf{T}_n \mathbf{T}_n^\dagger \right) B(T_n),
\end{aligned}
\tag{17}
$$

where we can ignore the last term because it will be nil by the definition above. The pattern here is that of two expanding series with one delayed index between them. By defining

$$
\mathbf{P}_i = \mathbf{T}_n \mathbf{T}_{n-1} \mathbf{T}_{n-2} \cdots \mathbf{T}_i,
\tag{18}
$$

the outgoing radiation of the last layer can be simplified as

$$
\mathbf{L}_{\text{out},n} = \mathbf{P}_1 \mathbf{P}_1^\dagger B_0 + \sum_{i=1}^{n-1} \left[\left(\mathbf{P}_{i+1} \mathbf{P}_{i+1}^\dagger - \mathbf{P}_i \mathbf{P}_i^\dagger \right) B(T_i) \right],
\tag{19}
$$

or even as

$$
\mathbf{L}_{\text{out},n} = \sum_{i=0}^{n-1} \left[\left(\mathbf{P}_{i+1} \mathbf{P}_{i+1}^\dagger - \mathbf{P}_i \mathbf{P}_i^\dagger \right) B(T_i) \right],
\tag{20}
$$

if we presume no transmission or reflection from the surface ($\mathbf{T}_0 = \mathbf{0}$), and that the surface is a blackbody with temperature T_0. These two assumptions

5

must be true for the extraction of B_0 to work in anyway, so Equation 20 is a valid simplification at this stage. The effective transmission from a layer is thus

$$\tau_{x,i} = \left. \mathbf{P}_{i+1}\mathbf{P}_{i+1}^{\dagger} \right|_x,\tag{21}$$

where x means that the end product (not the multiplication) is chosen for a select polarization state. Note that for the scalar case, this would be the exact transmission but that it can only be considered the effective transmission in matrix form because of the underlying assumption that, at the beginning of the path, the radiation was unpolarized. From the above we can find that $\Delta\tau(T_i, \cdots) = \tau_{x,i} - \tau_{x,i-1}$ in RTTOV. If the coherency matrices are in circular polarization basis as by Rosenkranz and Staelin (1988), then, e.g., the element on row two in column two represent left circular polarization.

Getting an effective transmission value for a polarized signal out of Stokes formalism is almost as straightforward as for coherency formalism. Taking the approach and assumptions of Equations 14 to 17 in Stokes formalism, radiation going out of the first layer is

$$\vec{I}_{\text{out},1} = \mathbf{C}_1\vec{B}_0 + [\mathbf{1} - \mathbf{C}_1]\,\vec{B}(T_1),\tag{22}$$

where $\exp(-\mathbf{K}_i r_i) \equiv \mathbf{C}_i$ the radiation leaving the second layer is

$$\begin{aligned}
\vec{I}_{\text{out},2} =& \mathbf{C}_2\mathbf{C}_1\vec{B}_0 + \\
& [\mathbf{C}_2 - \mathbf{C}_2\mathbf{C}_1]\,\vec{B}(T_1) + \\
& [\mathbf{1} - \mathbf{C}_2]\,\vec{B}(T_2),
\end{aligned}\tag{23}$$

the radiation leaving the third layer is

$$\begin{aligned}
\vec{I}_{\text{out},3} =& \mathbf{C}_3\mathbf{C}_2\mathbf{C}_1\vec{B}_0 + \\
& [\mathbf{C}_3\mathbf{C}_2 - \mathbf{C}_3\mathbf{C}_2\mathbf{C}_1]\,\vec{B}(T_1) + \\
& [\mathbf{C}_3 - \mathbf{C}_3\mathbf{C}_2]\,\vec{B}(T_2) + \\
& [\mathbf{1} - \mathbf{C}_3]\,\vec{B}(T_3),
\end{aligned}\tag{24}$$

and the outgoing radiation of the last layer is

$$\begin{aligned}
\vec{I}_{\text{out},n} =& \mathbf{C}_n\mathbf{C}_{n-1}\cdots\mathbf{C}_3\mathbf{C}_2\mathbf{C}_1\vec{B}_0 + \\
& [\mathbf{C}_n\cdots\mathbf{C}_2 - \mathbf{C}_n\cdots\mathbf{C}_1]\,\vec{B}(T_1) + \\
& [\mathbf{C}_n\cdots\mathbf{C}_3 - \mathbf{C}_n\cdots\mathbf{C}_2]\,\vec{B}(T_2) + \\
& [\mathbf{C}_n\cdots\mathbf{C}_4 - \mathbf{C}_n\cdots\mathbf{C}_3]\,\vec{B}(T_3) + \\
\cdots\;& [\mathbf{C}_n\cdots\mathbf{C}_{i+1} - \mathbf{C}_n\cdots\mathbf{C}_i]\,\vec{B}(T_i) + \\
\cdots\;& [\mathbf{1} - \mathbf{C}_n]\,\vec{B}(T_n),
\end{aligned}\tag{25}$$

where we again can ignore the last term for it is nil. If we, as for Amsutran, define a matrix product

$$\mathbf{D}_i = \mathbf{C}_n \mathbf{C}_{n-1} \mathbf{C}_{n-2} \cdots \mathbf{C}_i, \tag{26}$$

then the outgoing radiation of the last layer can be simplified

$$\vec{I}_{\text{out},n} = \sum_{i=0}^{n-1} \left[(\mathbf{D}_{i+1} - \mathbf{D}_i) \, \vec{B}(T_i) \right], \tag{27}$$

which always is equivalent to Equation 20, if the spectroscopic input and atmospheric layering is the same for the two formalisms. The effective transmission equivalent as in Equation 21 is slightly more difficult to extract since it requires the vector multiplication

$$\tau_{x,i} = \left. \mathbf{D}_{i+1} \left[1, 0, 0, 0 \right]^\top \right|_x, \tag{28}$$

where, since the vector is of length one, e.g., the left circular polarization effective transmission is from addition of the first and last element of the resulting vector.

Theoretical Differences in Zeeman Treatment. ARTS and Amsutran are very similar in their theoretical treatment of the Zeeman effect for the lines of interest. The only physical differences I have identified from the work by Rosenkranz and Staelin (1988) to the work in ARTS is that the radiation is rotated per level to always be in sensor polarization coordinate system (in their Equation 1, the rotation is performed by the ρ-matrices), and that ARTS use the relativistic correction for non-free electrons (for details on this correction, see Christensen and Veseth, 1978). The former should only matter for linear polarization, and the latter should only change 1/5000 of the broadening. Another difference is that ARTS works with either a full or constant magnetic field, whereas Amsutran only works with a constant field (i.e. 3D or 2D look-up table). The changing field effect is difficult to quantify except by running the full ARTS v. ARTS with limited magnetic field.

3 Data

The models are given identical profiles in all simulations. Profiles are assumed to consist of pressure-gridded temperature, H_2O volume mixing ratio (VMR), N_2 VMR, and O_2 VMR. The same formula as used internally in RTTOV is used to also provide ARTS with its required height-grid. Both O_2 and N_2 are assumed of constant mixture throughout this comparison, although I want to point out that there are issues with this above $\sim$1 Pa.

The profiles used for the direct model comparisons are hybrids of the profiles that were used by Han et al. (2007) and the profiles (with more levels in the troposphere) used to train RTTOV for non-Zeeman channels. As I understand the hybridization process, it has not altered the radiative transfer output for channels 19-22. I will therefore throughout this work refer to these profiles as the training profiles. There are 52 profiles in this set. The last three profiles in the list of 52 are special. Profile number 52 is the mean of the other 49 profiles, profile number 51 is the maximum of the other 49 profiles, and profile 50 is the minimum of the other 49 profiles. The range of pressure, temperature and height encompassed by these profiles is plotted in Figure 1. There is a small change in water vapor content and O_3 content with height, though these molecules are only indirectly important for this study and can mostly be ignored. For the effective transmission comparison, and for the angular dependency comparison, only the mean profile was used.
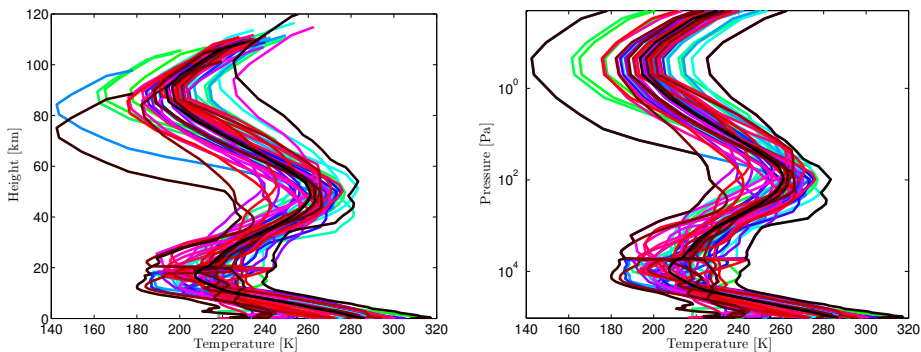

Figure 1: Atmospheric temperatures used in the model comparison simulations. These corresponds to the profiles Amsutran used to train RTTOV.

There are 24 SSMIS channels. I only worked to compare channels 19-22. These give information about in the upper atmosphere, and are affected by the Zeeman effect. The pass-bands of the channels are in Table 1. The response function of these channels are given in Figure 3 for the average profile of Figure 1.

There are no differences between Amsutran and ARTS line data. This was ensured by the models using the same line strengths, central frequencies, and pressure broadening parameters for the relevant lines. These line data are found in Table 2. ARTS is run fully ignoring line mixing. Amsutran is ignoring line mixing for pressures less than 12 hPa, and RTTOV ignores it altogether when using the Han coefficients. Virtually all information from the SSMIS channels are from levels with pressure less than 12 hPa.

Comparison with SSMIS data were attempted. The profiles in these comparisons are from model output prepared by *Booton*. The magnetic field model used is from Finlay et al. (2010), and is named the International

Channel	Pass-band	Lower Limit	Upper Limit
19			
	1	62 997.30 MHz	62 998.66 MHz
	2	63 567.84 MHz	63 569.20 MHz
20			
	1	60 434.10 MHz	60 435.45 MHz
	2	61 149.88 MHz	61 151.23 MHz
21			
	1	60 432.13 MHz	60 433.42 MHz
	2	60 436.13 MHz	60 437.42 MHz
	3	61 147.91 MHz	61 149.20 MHz
	4	61 151.91 MHz	61 153.20 MHz
22			
	1	60 427.97 MHz	60 430.59 MHz
	2	60 438.97 MHz	60 441.59 MHz
	3	61 143.75 MHz	61 146.37 MHz
	4	61 154.75 MHz	61 157.37 MHz

Table 1: SSMIS channels used in the simulations. The SSMIS channels are centered between two lines. The pass-bands are split so that each pass-band of a channel measures spectroscopically similar parts of the lines.

Line	Line Strength	Line Center	Pressure Broadening
7+	3.956001×10^{-19} Hz m^2	60 434.8 MHz	13 110.028 Hz/Pa
9+	4.058198×10^{-19} Hz m^2	61 150.6 MHz	12 614.738 Hz/Pa
15+	2.477872×10^{-19} Hz m^2	62 998.0 MHz	11 512.970 Hz/Pa
17+	1.797588×10^{-19} Hz m^2	63 568.5 MHz	11 199.623 Hz/Pa

Table 2: Line data used in simulations. These are for $T_0 = 296$ K reference temperature. The pressure broadening temperature scaling is $(T_0/T)^{0.8}$. The line strength in ARTS scales with the total integrated partition sums of Fischer and Gamache (2002), which might have been updated since it was first published. Amsutran/RTTOV scales similarly with temperature, though only partitions the strengths based on the energy levels' angular momentum.

Geomagnetic Reference Field 11 (IGRF-11). ARTS is run with both the full magnetic field model and a constant magnetic field extracted at ~5 Pa. RTTOV is run with the same extracted magnetic field. The magnetic field angle for the constant field is calculated for a geometrical propagation path from the ground to the satellite. Taking refraction into account would give a more proper magnetic angle, but the difference is small, and similarly small is the resulting change in Zeeman effect line shape. The radiative transfer calculations do not assume geometrical propagation path, this was

only used to extract the constant magnetic field. The constant magnetic field strengths and magnetic field angles used in this comparison can be found in Figure 2. In this figure, and throughout this report, θ is the angle between the magnetic field and the propagation direction vector for the radiation, and H is the magnitude of the magnetic field.

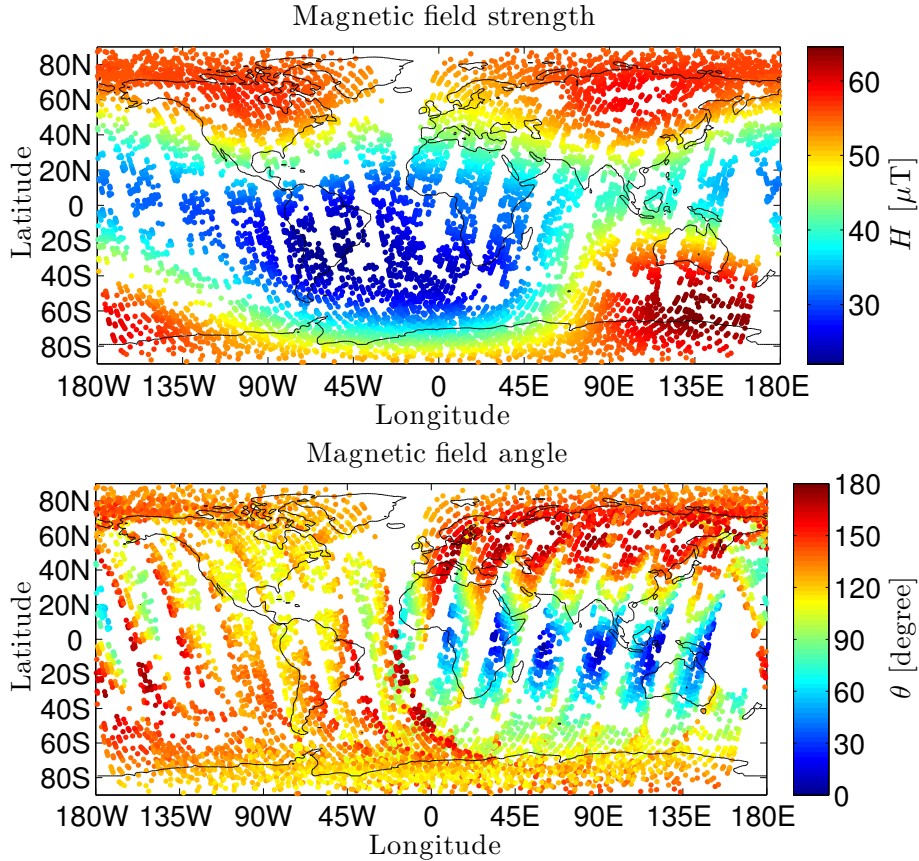
Figure 2: Magnetic field used in RTTOV simulations. These are based on IGRF-11 for an approximated height of 5 Pa. To the left is the field strength and to the right is the corresponding field angle relative to the propagation path of the radiation assuming geometrical propagation path from the ground to the satellite.

For all direct model comparisons (i.e. when only ARTS and Amsutran/RTTOV are involved without SSMIS data), I assume a constant magnetic field strength and angle throughout the propagation in both models.

4   Results

Effective Transmission.   Figures 4 to 7 show effective transmission for channels 19 to 22, respectively, for nadir geometry comparing ARTS and Amsutran for the mean profile in Figure 1. The effective transmission is defined by Equations 21 and 28 for either left or right circular polarisation — when, as here, Doppler shifts are ignored, SSMIS channels will symmetrical about O_2 lines, and the sense of polarisation will be immaterial. Off-nadir calculations were performed, and are virtually identical to the nadir effective transmission figures so they are left out of this report. (Since Amsutran is plane parallel, the effective transmission calculations have to be performed in post-processing of ARTS simulations to minimize model differences. These post-processing were done from level-by-level point-values of **K**, manually creating the plane parallel atmospheric structure to match Amsutran exactly.)

Channel 22 effective transmission (Figure 7) does not change with changing magnetic field strength and angle. Channel 21 effective transmission (Figure 6) changes strongly for increasing magnetic field strength when the angle is not 90°, in which case the change in effective transmission is small. Channel 20 effective transmission (Figure 5) changes strongly for increasing magnetic field strength when the angle is not 90° in which case the change in effective transmission is smaller but still noticeable in the plots. Channel 19 effective transmission (Figure 4) changes weakly for increasing magnetic field strength.

Brightness Temperature.   Figures 8 to 11 shows brightness temperature simulations for channels 19 to 22, respectively, for both ARTS and RTTOV. The observation geometry is as for SSMIS (around 55° angle for the radiation path to the normal of the surface), and all profiles in Figure 1 are used in the simulations. The plots contain information about how well ARTS and RTTOV agree in the form of R^2 and bias value. These two values have been calculated following the assumption that there should be a one-to-one match between the models, i.e. that for the simulated brightness temperature

$$T_b^{[\text{RTTOV}]} = T_b^{[\text{ARTS}]} + T_b^{[\text{bias}]}(H, \theta), \qquad (29)$$

and the agreement with the linear model has been defined as the squared residual divided by the variance times the number of data points, i.e.

$$R^2 = 1 - \frac{\sum_{i=1}^{N} \left[T_{b,i}^{[\text{RTTOV}]} - \left(T_{b,i}^{[\text{ARTS}]} + T_b^{[\text{bias}]}(H, \theta) \right) \right]^2}{\sum_{i=1}^{N} \left[T_{b,i}^{[\text{RTTOV}]} - \left\langle T_b^{[\text{RTTOV}]} \right\rangle \right]^2}, \qquad (30)$$

where $\left\langle T_b^{[\text{RTTOV}]} \right\rangle$ is the average of $T_b^{[\text{RTTOV}]}$.

Channel 22 brightness temperature (Figure 11) has a negative bias of between 0.8 K and 1 K, with a constant $R^2 = 0.990$ in the plots. Channel 21 brightness temperature (Figure 10) has a positive bias of between 1 K and 3 K, with R^2 ranging from 0.981 at worst to 0.993 as best in the plots. Channel 20 brightness temperature (Figure 9) has a positive bias of between 3 K and 6 K, with R^2 ranging from 0.994 at worst to 0.999 as best in the plots. Channel 19 brightness temperature (Figure 8) has a positive bias of between 4 K and 5 K, with R^2 ranging from 0.977 at worst to 0.992 as best in the plots.

Angular Dependency. Figure 12 shows how the mean bias changes between ARTS and RTTOV as a function of magnetic field angle for the mean profile in Figure 1 for a weak magnetic field (20,000 nT) and for a strong magnetic field (70,000 nT). Channel 22 bias is practically constant for all angles, but shows a strange numerical error that is especially prominent when the magnetic field is weak. Channel 21 bias changes by about 25% of the mean bias as a function of magnetic angle for a weak magnetic field, and by nearly 100% of the mean bias when the magnetic field is strong. Channel 20 bias changes by 80% of the mean bias when the magnetic field is weak, and by 40% of the mean bias when the magnetic field is strong. Channel 19 bias does not change much with angle compared to its mean bias.

SSMIS Direct Comparison. Figures 13 and 14 shows a global comparison of ARTS and RTTOV taking measurement from SSMIS into account for the four channels. In these plots, the top-most plot is the raw data returned by SSMIS, second row from the top is RTTOV simulations, third is ARTS simulations, fourth is the comparison between ARTS and RTTOV (ARTS simulation minus RTTOV simulation), fifth is the comparison between RTTOV and SSMIS (RTTOV simulation minus SSMIS data), and the last row is the comparison between ARTS and SSMIS (ARTS simulation minus SSMIS data). The profiles of these simulations are output by the Met Office Numerical Weather Prediction model (NWP). The magnetic field used by ARTS is the full IGRF-11 model, whereas RTTOV uses the magnetic field of Figure 2. All atmospheric state parameters of interest are considered constant from and above 10 Pa, which is the highest level of the stored atmospheric profile [N.B. no NWP model goes higher than this], up to and including the pressure that is the top-of-the-atmosphere in Figure 1. Figure 15 is the model comparison between ARTS and RTTOV when ARTS is run with the same constant magnetic field as RTTOV.

5   Discussion and Conclusions

Channel 22   is the lowest of the four channels. It is thus the channel least affected by the Zeeman effect. That it is barely concerned with the Zeeman effect is shown in its effective transmission (Figure 7). There is practically no change in effective transmission for channel 22 with changing magnetic field strength and magnetic field angle, and in turn no practical differences between ARTS and RTTOV for changing magnetic angle (Figure 12). There is, however, a large discrepancy between Amsutran and ARTS effective transmission for this channel. In Figure 11, this difference in effective transmission shows up as a difference in brightness temperature of about 1 K between ARTS and RTTOV. The same order of difference shows up in Figure 14 when comparing with SSMIS input profiles (that are cut off at 10 Pa). It is difficult to pinpoint the cause of the difference since the models are run using the same atmospheric input, and the same spectroscopic parameters. The difference is however not caused by differing treatment of the Zeeman effect. I strongly suspect it is caused by a difference in how the homogeneous layers are created. ARTS averages spectroscopic parameters (i.e. $\mathbf{K}$ and $\vec{B}(T)$) from two surrounding levels, whereas Amsutran/RTTOV averages physical parameters (i.e. p and T) before calculating the spectroscopic parameters. In ideal conditions, e.g. when a profile is very narrowly gridded, the different layering methods of ARTS and RTTOV should not make a difference, but in this particular case the gridding is not narrow (as can be seen by the shape of Figure 1 for higher altitudes, where there are sometimes 10 km between levels).

From Figure 14 it seems ARTS is better at describing channel 22. The differences between the models are significant, because the mean bias is on the same order as is the variation ($\sim$1 K). However, the variation in the comparison between data and model ($\sim$6 K) is much larger than the variation between the models, so it is difficult to say whether ARTS or RTTOV is the better model. Keeping the magnetic field constant does not make a large difference for this channel (as seen from comparing Figures 15 and 14).

Channel 21   is higher than channel 22, but not by much. It is consequently more affected by the magnetic field, but not by much. This is seen in Figure 6, where the change in effective transmission over altitude is much smaller for angles 0° and 180° for the strong magnetic field than it is for the weaker magnetic field. (That there is almost no change in effective transmission when the magnetic angle is close to 90° is because this angle causes a more symmetric line shape around the line center, which in turn hides the Zeeman effect better at low pressures.) From Figure 12, at these higher magnetic field strengths it becomes clear that there is a difference in treatment of the Zeeman effect for channel 21 between the models. Since in Figure 12, the average bias between the models ($\sim$2 K) is similar in size as

the change with angle ($\sim$1.5 K). In Figure 10, the bias between the models in brightness temperature is about 2 K. Even though there are large changes in the bias with the changing angle, this could be an enhancement of the layer problem when the transmission is changing.

From Figure 14 it seems RTTOV is better at describing channel 21. However, in contrast to channel 22, the variation between the models is larger than the bias between the models, so it is difficult to say which model is better. Also, as for channel 22, the variation in the data is much larger than the variation between the models, which makes it even more difficult to tell which model is more correct. Note that in Figure 14 the average bias between the models is much smaller than for the training profiles (0.5 K v. 2 K). This enforces the idea that large parts of the bias between the models is caused by how the models define a layer. Keeping the magnetic field constant does not make a large difference for this channel (as seen from comparing Figures 15 and 14).

Channel 20 is the highest of the four channels. It is strongly affected by the Zeeman effect. This is seen in Figure 5, where it is clear that there is a difference between how ARTS and Amsutran treats the Zeeman effect. The difference in response function between the models changes a lot for different magnetic fields, most out of the four channels. This is seen in the large variation of brightness temperature bias in Figure 9. Despite the having the largest changes in response function for magnetic field changes of the four channels, the R^2 for a one-to-one match between the models is also the highest out of the four channels. The average bias in Figure 12 is much larger than the variation for channel 20. The high R^2 between ARTS and RTTOV combined with the large differences between ARTS and Amsutran transmissions are very puzzling. Somehow, despite the transmission that changes with magnetic angle and magnetic field strength, only a constant bias emerges between the models.

From Figure 13 neither model can describe the raw SSMIS data for channel 20. This is not surprising since the profile is cut off well below the peak of the channel response function. The models, on the other hand, agree well with each other in mean difference but not in variation. Looking in detail on these plots, the variation between the models is mainly caused by differing angular dependencies. (This can be seen, e.g., by looking at one swath near the equator, where the models agree well in the middle of the swath, but has positive or negative biases on altering sides of the middle. Since at the equator the magnetic angle changes the most over a swath, and this is where we see the largest biases, it is clear that the cause is that RTTOV and ARTS behave different for different angles.) Keeping the magnetic field constant in ARTS (Figure 15) makes a large difference for channel 20, compared to using the full magnetic field (fourth row of

14

Figure 13). The average bias between the models do not change much, but the angular dependency is reduced strongly, and as a consequence there is much less variation between the models.

Channel 19 is the second highest of the four channels. It is strongly affected by the Zeeman effect. This is seen in Figure 4, where it has a consistently much lower change in transmission with altitude than, e.g., channel 22. The effective transmission of channel 19 seems to agree better than for all the other channels, regardless of magnetic field strength and angle. Channel 19 still has one of the largest model-to-model bias for the training profiles (Figure 8). It shares this high bias only with channel 20. However, channel 19 bias has a much smaller dependency on angle than channel 20 (Figure12). In contrast to channel 20, channel 19 has the most variation in its R^2 but the model differences in transmission seems to be very stable and low.

For the same reason as given for channel 20, from Figure 13 neither model can describe the raw SSMIS data for channel 19. Still, the model agree very well with each other, but (again as for channel 20) there is a large difference over a single swath between the models. Keeping the magnetic field constant in ARTS (Figure 15) makes a large difference for channel 19, compared to using the full magnetic field (fourth row of Figure 13). The average bias between the models is not changed by much, but the angular dependency is reduced strongly, and as a consequence there is much less variation between the models.

Layer Treatment. It is clear that there is an issue in how the radiative transfer codes treat layers. Both of the definitions from the theoretical sections should yield similar results if the atmospheric profile is homogeneous. The atmospheric profiles stored with SSMIS data only go up to 10 Pa and have here been extrapolated at constant temperature. Therefore, the profiles are constant for the high-peaking channels 19 and 20 of Figure 15, but it is not constant for the lower peaking channels 21 and 22. Since the bias between the models is much smaller in the channels with the constant profiles than the bias in Figures 8-11, I think this layering difference is responsible for large parts of the simulated differences in brightness temperature. It is important to work out ways to better produce homogeneous layers for RTTOV.

Angular and Strength Bias. The assumption that a bias (as a function of channel, magnetic field strength and magnetic angle) and the simulation of one model is all that is necessary to accurately tell what the other model will simulate seems good. There is a constantly high R^2 for all channels despite the identified differences in layer treatment and angular dependencies. Part

of the bias is likely caused by the differences in the treatment of the Zeeman effect. E.g., Figure 13 shows that when the profile is constant (i.e. there is minimal difference between how the models define their layers), then the bias is nil near center of the swath. This bias diverges a lot from one side of the swath to the next, however this divergence is reduced in Figure 15 where the magnetic field in ARTS is constant. The last point seems to indicate that the angular bias is caused by not allowing for the magnetic field to change, however Figure 12 seems to indicate that there is still an underlying issue with angular dependency in the bias. Perhaps Figure 12 is enhancing the issues caused by the layering, because combining Figures 13 and 15 definitely show that the changing magnetic field is an important different between the models.

On Numerical Accuracy. One thing I find interesting is the question of numerical accuracy. It is clear that the channels of Table 1 are intended to be centered around the four lines of Table 2. For example, channel 19 is centered at the 15+ and 17+ lines. Looking at these tables, however, we are not modeling line-centered pass-bands. The reason this is not the case in the tables is that Amsutran, and therefore RTTOV, are using line data that is only accurate to within 100 kHz, whereas SSMIS are centered on the lines to an accuracy of 10 kHz. The channels are about 3 MHz wide for channel 19, so the difference in line center could be important. Since the coefficients used by RTTOV were derived by Han et al. (2007) and not by Amsutran, these biases might be included in the simulated results described throughout this report. (I do not know what line parameters *Yong Han* used to derive his coefficients.)

On the Response Functions. Figure 3 show that some channels are influenced by the top-most parts of the average profile. This might be problematic, since it could indicate that there are absorption/emission above the profile.

Short List Conclusion list:

- There is a difference in layer definition that likely causes large biases between the models.

- There is a difference in response with angle in Zeeman-affected spectra. Major parts of this difference in response is caused by using a constant magnetic field in RTTOV. Allowing the magnetic field to change throughout propagation could be important.

- In no way is the profiles used for SSMIS in NWP reaching high enough to model the higher peaking SSMIS channels. This makes it difficult to tell which model better represent the data.

- A model bias as a function of magnetic field strength and angle is sufficient to accurately predict the simulation results of one model c.f. the other model even with the layer issue and angular dependency.

- We are not accurately modeling line-centered pass-bands with the present spectroscopy.

- To take all the atmospheric absorption/emission effects into account, the training profiles should go higher (to lower pressures) than is currently the case.

6 Future Work

The ability to generate RTTOV coefficients at the Met Office is necessary for my recommendations. Luckily, by 2014-04-15 *Rayer* confirmed that this was now possible. The newly generated coefficients had a small impact on the simulated results of this report but were not studied in detail.

My major recommendations for RTTOV-12:

Refine the profiles to be have more layers. This might require increasing the number of pressure bins by which the training profile is run. Most of the differences between ARTS and RTTOV are likely caused by the way layers are treated.

Identify a way to counteract the differences that occur because the magnetic field is physically changing throughout propagation (c.f. Figures 15 and 13). This recommendation is perhaps more geared towards NWP models than for RTTOV-12, but since it affects the physical spectra I include it here. For NWP, the bias as a function of the magnetic field between ARTS and RTTOV is a good starting point since it should be simple to implement. For RTTOV, major work to derive predictors that allow for a changing magnetic field would be required. I am not sure this is possible withing the present structure of RTTOV. Discussion with *Rayer* indicate it might be difficult to supply the field variables at run-time (i.e. operationally), but neither of us put much thought on this point.

Unknown impact:

Increase accuracy of line centers in Amsutran. It should be safe to simply replace these values with, e.g., the more accurate JPL line centers. This would help by increasing accuracy of simulations by more accurately centering the channel pass-bands evenly around the line center. The problem with the values used at present is that the line centers are only accurate to ± 50 kHz, whereas the channels are accurate to ± 5 kHz. Since the channels are only a few MHz wide,

this accuracy issues could be important when working with SSMIS data. I have not quantified how important these accuracies are for the simulated result, so the impact is unknown.

Increase the top-of-the-atmosphere height. There might be more absorption above the present limits. I am not sure how important this is for the transfer simulation, but it should be kept in mind while revisiting the training profiles that the top-of-the-atmosphere is low compared to the response functions with the present upper pressure limit.

Minor recommendation:

Replace ABC/2.8026E-3/ with ABC/2.8022E-3/ in Amsutran zeeman.f. This is equivalent to updating g_s from 2.00232 to 2.002089. The former is the correction term for relativistic free electrons used by Lenoir (1967, 1968), and the latter is the theoretical value reported in Christensen and Veseth (1978) for O_2. Christensen and Veseth (1978) also reported measurements of $g_s = 2.002064$, which if true means that ABC/2.8021E-3/ should be used. I recommend to use the theoretical value because a single measurement is difficult to trust. (This would only increase accuracy of the Zeeman broadening by a very small amount.)

Notes from discussions that did not make it into the report:

- Discussion with *Rayer*. The coefficients by Amsutran should be generated on evenly spaced θ.

- Discussion with *Bell*. The models agree within the limit of instrumental error. If the simulations are accurate, using RTTOV to simulate the temperature would greatly improve on present methods in NWP where no Zeeman effect is included in the simulations. This is regardless of whether ARTS or RTTOV are better at representing the channel values.

- General discussion. I think it is possible to include the direction of the magnetic field in the plane of the propagation of the radiation to generate linearly polarized effective transmission. This would improve on AMSU-A theory, which presently simulates the average of vertical and horizontal polarizations in the sensor scan plane (*Rayer*, personal communication).

References

H. Christensen and L. Veseth. On the high-precision Zeeman effect in O_2 and SO. *Journal of Molecular Spectroscopy*, 72(3):438–444, 1978. doi: 10.1016/0022-2852(78)90142-X.

J. C. del Toro Iniesta. *Introduction to Spectropolarimetry.* Cambridge University Press, 2004.

C. C. Finlay, S. Maus, C. D. Beggan, T. N. Bondar, A. Chambodut, T. A. Chernova, A. Chulliat, V. P. Golovkov, B. Hamilton, M. Hamoudi, R. Holme, G. Hulot, W. Kuang, B. Langlais, V. Lesur, F. J. Lowes, H. Lühr, S. Macmillan, M. Mandea, S. McLean, C. Manoj, M. Menvielle, I. Michaelis, N. Olsen, J. Rauberg, M. Rother, T. J. Sabaka, A. Tangborn, L. Tffner-Clausen, E. Thébault, A. W. P. Thomson, I. Wardinski, Z. Wei, and T. I. Zvereva. International geomagnetic reference field: the eleventh generation. *Geophysical Journal International*, 183:1216–1230, September 2010.

J. Fischer and R. R. Gamache. Total internal partition sums for molecules of astrophysical interest. *Journal of Quantitative Spectroscopy and Radiative Transfer*, 74:263–272, 2002.

Y. Han, F. Weng, Q. Liu, and Paul van Delst. A fast radiative transfer model for SSMIS upper atmosphere sounding channels. *Journal of Geophysical Research*, 112:D11121, 2007. doi: 10.1029/2006JD008208.

S. Kobayashi, M. Matricardi, D. Dee, and Sakari Uppala. Toward a consistent reanalysis of the upper stratosphere based on radiance measurements from SSU and AMSU-A. *Quarterly Journal of the Royal Meteorological Society*, 135:2086–2099, 2009.

R. Larsson, S. B. Buehler, P. Eriksson, and J. Mendrok. A treatment of the Zeeman effect using Stokes formalism and its implementation in the Atmospheric Radiative Transfer Simulator (ARTS). *Journal of Quantitative Spectroscopy and Radiative Transfer*, 133:445–453, 2014.

W. B. Lenoir. Propagation of partially polarized waves in a slightly anisotropic medium. *Journal of Applied Physics*, 38(13):5283–5290, 1967.

W. B. Lenoir. Microwave spectrum of molecular oxygen in the mesosphere. *Journal of Geophysical Research*, 73(1):361–376, 1968.

P. W. Rosenkranz and D. H. Staelin. Polarized thermal microwave emission from oxygen in the mesosphere. *Remote Sensing*, 23(5):721–729, 1988.

P. Zeeman. On the influence of magnetism on the nature of the light emitted by a substance. *Philosophical Magazine*, 43:226, March 1897.
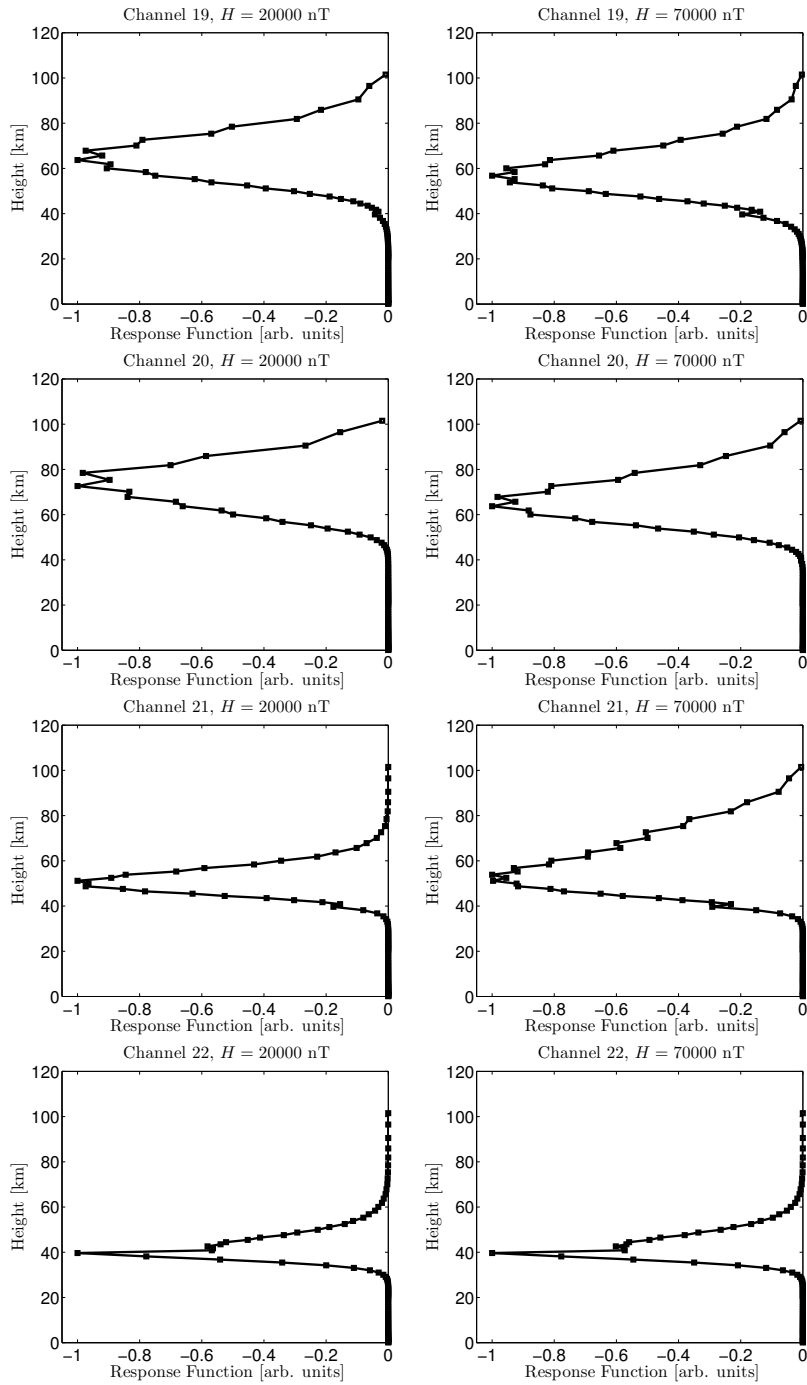
Plots

Figure 3: Response functions for all the channels in arbitrary units. This is a rescaled $\Delta\tau$ as defined by Equation 8. Only three magnetic angles have been used in computing these response functions before rescaling. These are 0°, 90 °, and 180°. The averaging is done on both ARTS and Amsutran simulations.
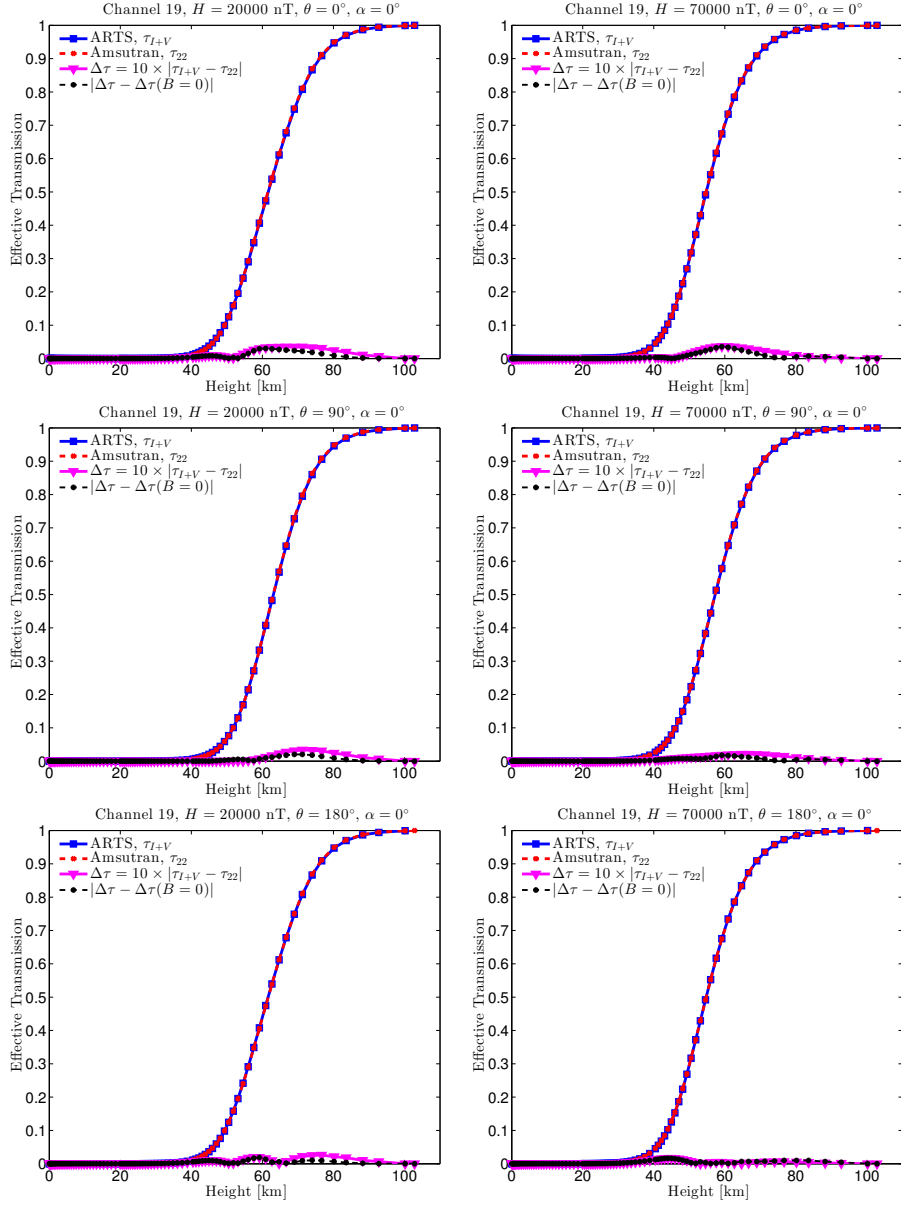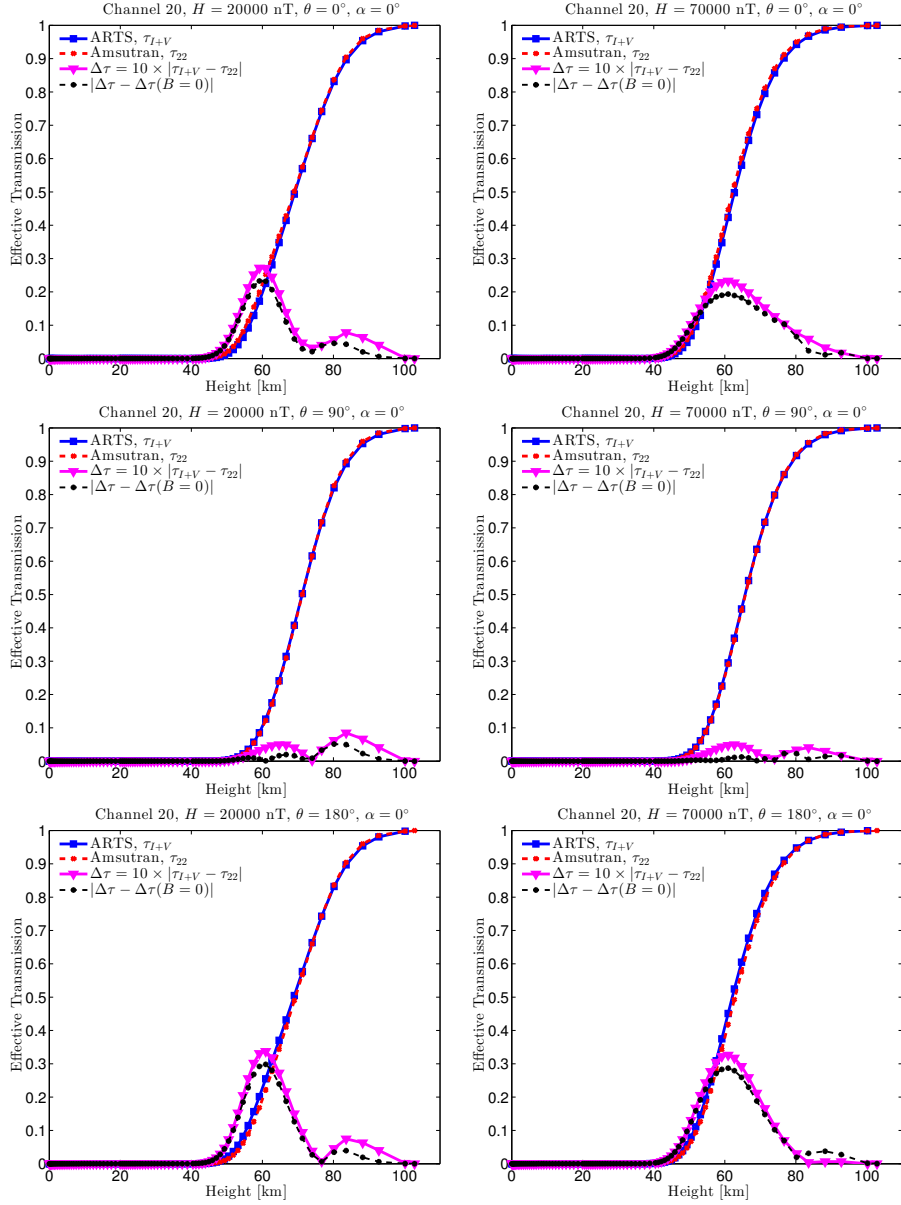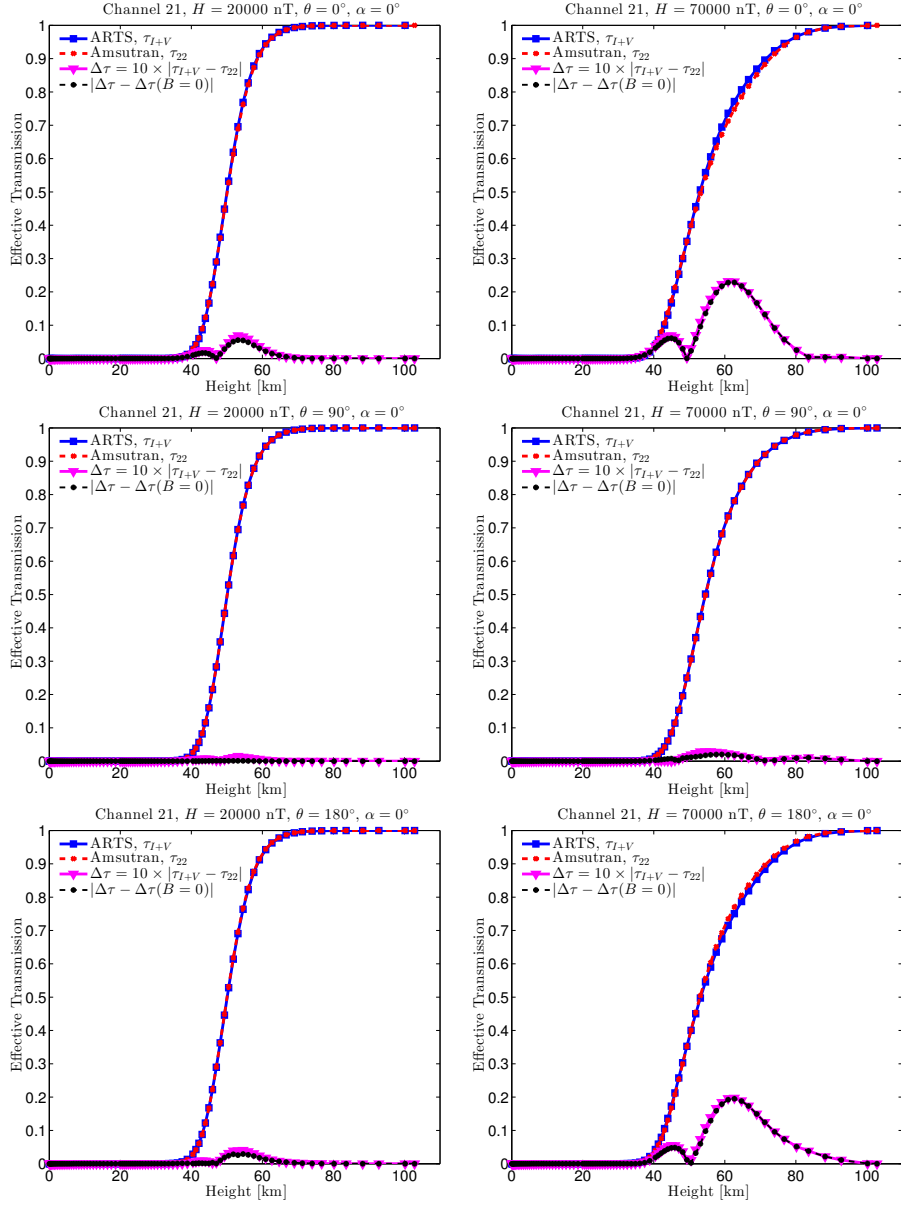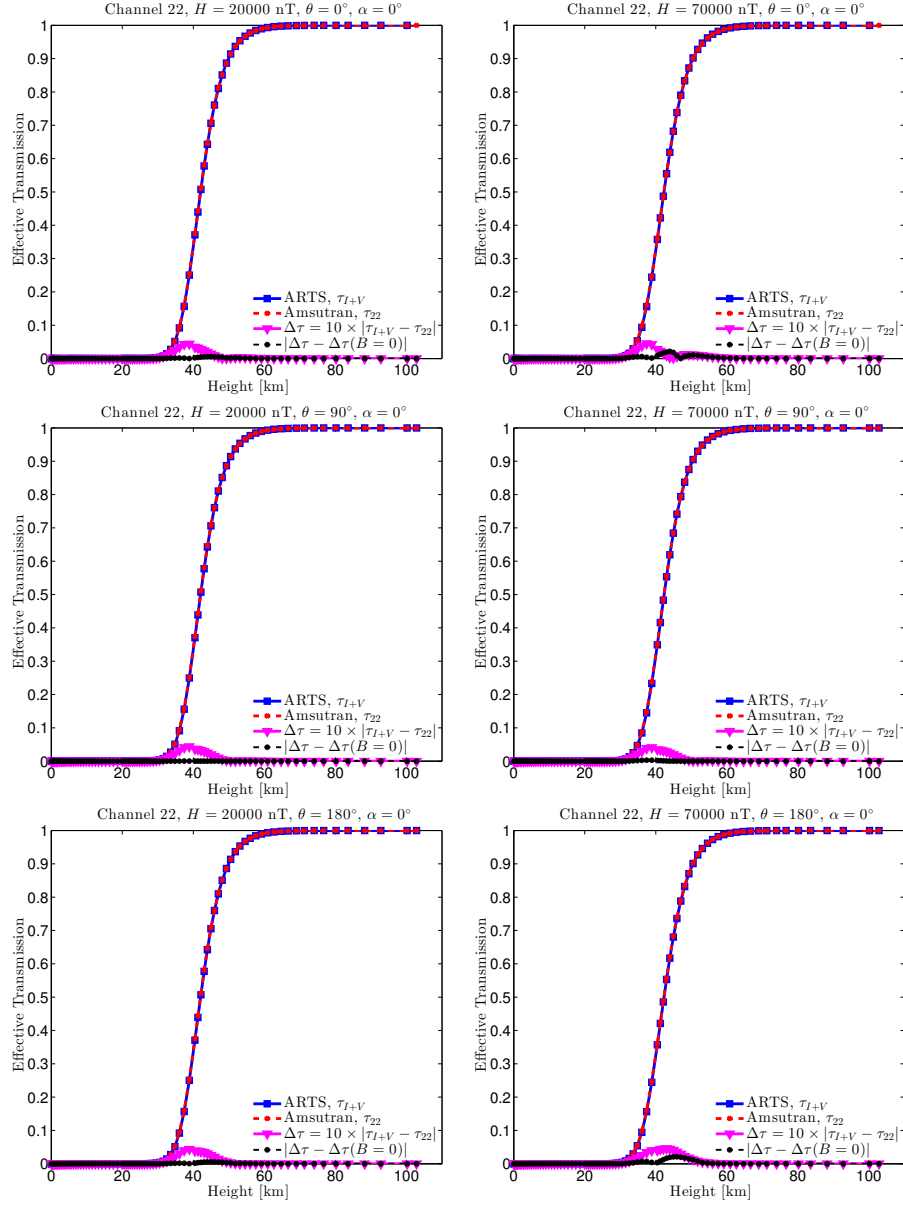
Figure 4: Channel 19 effective transmission for ARTS and Amsutran. The title of each plot contains magnetic field strength H, magnetic field angle relative to the propagation path θ, and zenith angle α. Only nadir is considered.

Figure 5: Channel 20 effective transmission for ARTS and Amsutran. The title of each plot contains magnetic field strength H, magnetic field angle relative to the propagation path θ, and zenith angle α. Only nadir is considered.

Figure 6: Channel 21 effective transmission for ARTS and Amsutran. The title of each plot contains magnetic field strength H, magnetic field angle relative to the propagation path θ, and zenith angle α. Only nadir is considered.

Figure 7: Channel 22 effective transmission for ARTS and Amsutran. The title of each plot contains magnetic field strength H, magnetic field angle relative to the propagation path θ, and zenith angle α. Only nadir is considered.
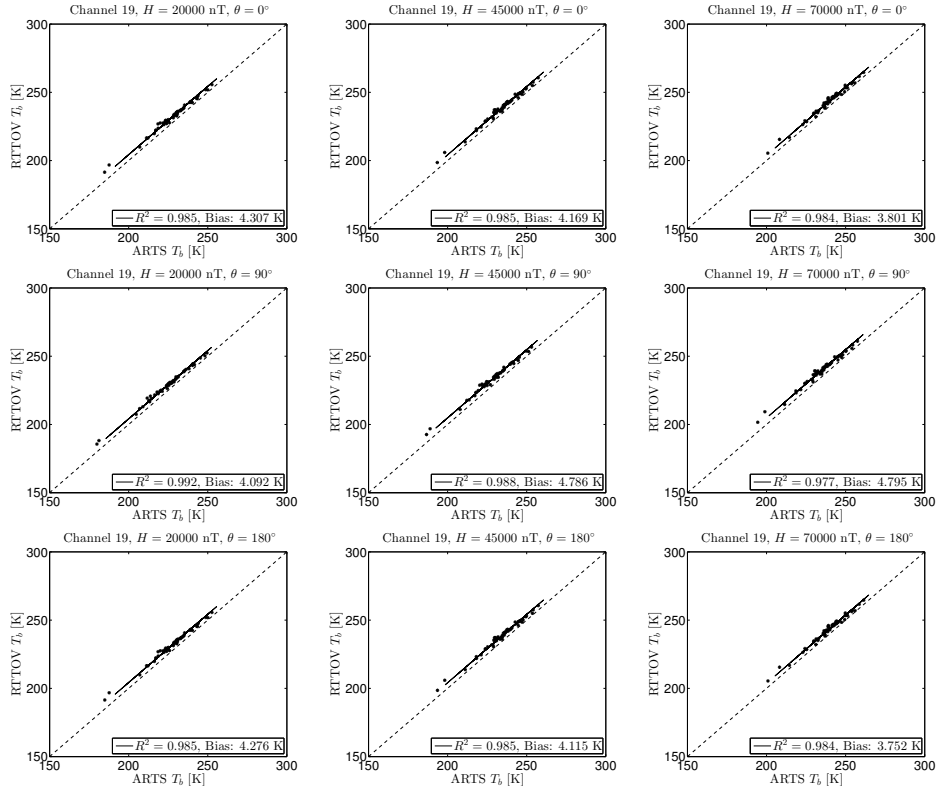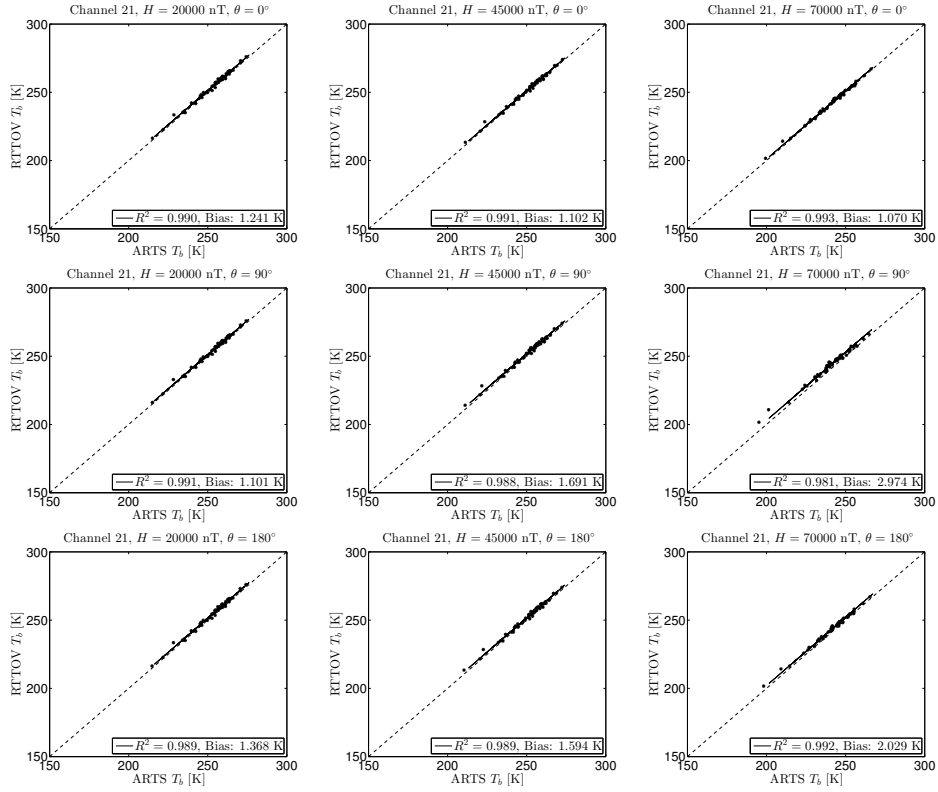
Figure 8: Channel 19 brightness temperature for ARTS and RTTOV. The plot title indicates magnetic field strength and magnetic field angle. Each plot contains 52 data points, one for each of the 52 training profiles used by Han et al. (2007) to train RTTOV. The bias and R^2 of a best-fit model is given in the legend. The R^2 is relative to a one-to-one fit with this bias, as described in the text.
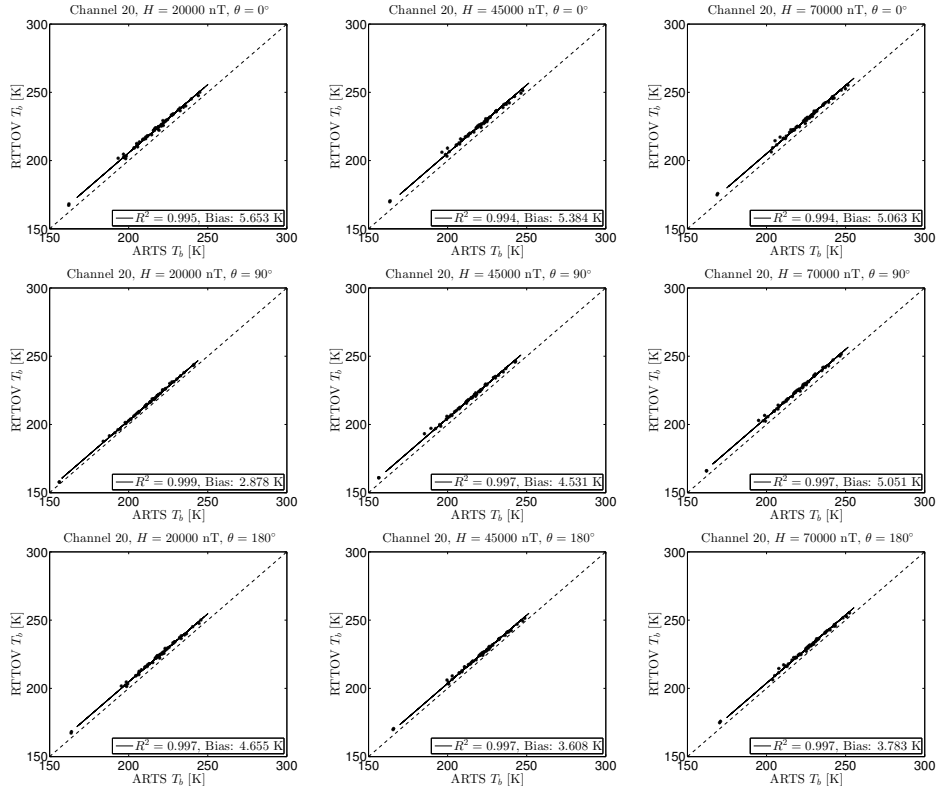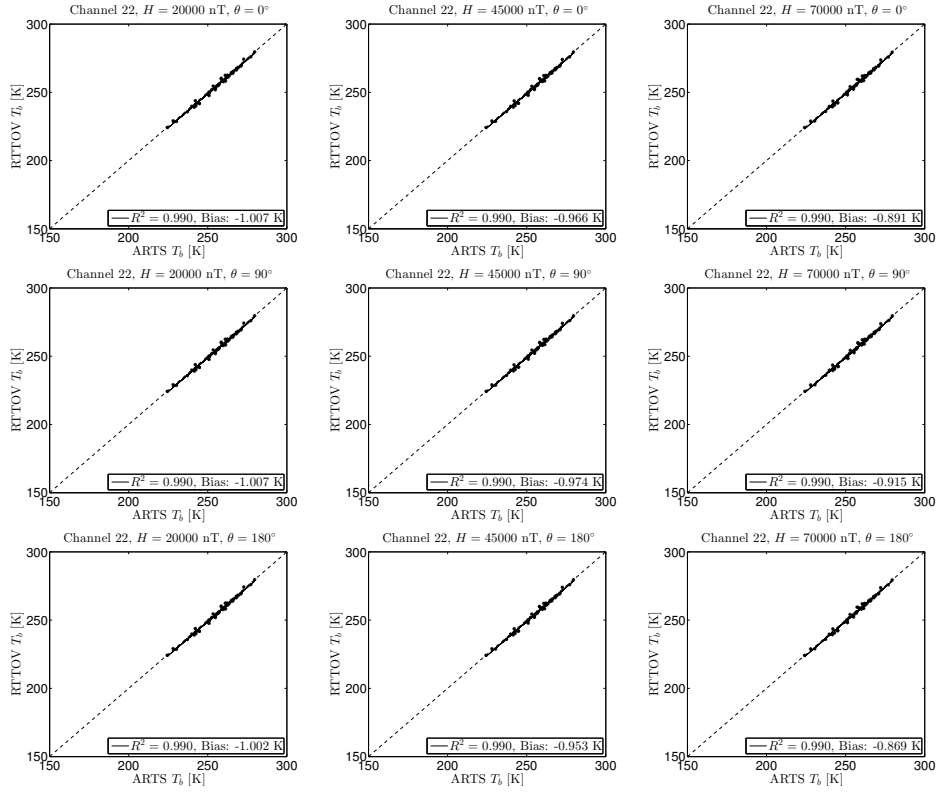
Figure 9: Channel 20 brightness temperature for ARTS and RTTOV. The plot title indicates magnetic field strength and magnetic field angle. Each plot contains 52 data points, one for each of the 52 training profiles used by Han et al. (2007) to train RTTOV. The bias and R^2 of a best-fit model is given in the legend. The R^2 is relative to a one-to-one fit with this bias, as described in the text.

Figure 10: Channel 21 brightness temperature for ARTS and RTTOV. The plot title indicates magnetic field strength and magnetic field angle. Each plot contains 52 data points, one for each of the 52 training profiles used by Han et al. (2007) to train RTTOV. The bias and R^2 of a best-fit model is given in the legend. The R^2 is relative to a one-to-one fit with this bias, as described in the text.

Figure 11: Channel 22 brightness temperature for ARTS and RTTOV. The plot title indicates magnetic field strength and magnetic field angle. Each plot contains 52 data points, one for each of the 52 training profiles used by Han et al. (2007) to train RTTOV. The bias and R^2 of a best-fit model is given in the legend. The R^2 is relative to a one-to-one fit with this bias, as described in the text.
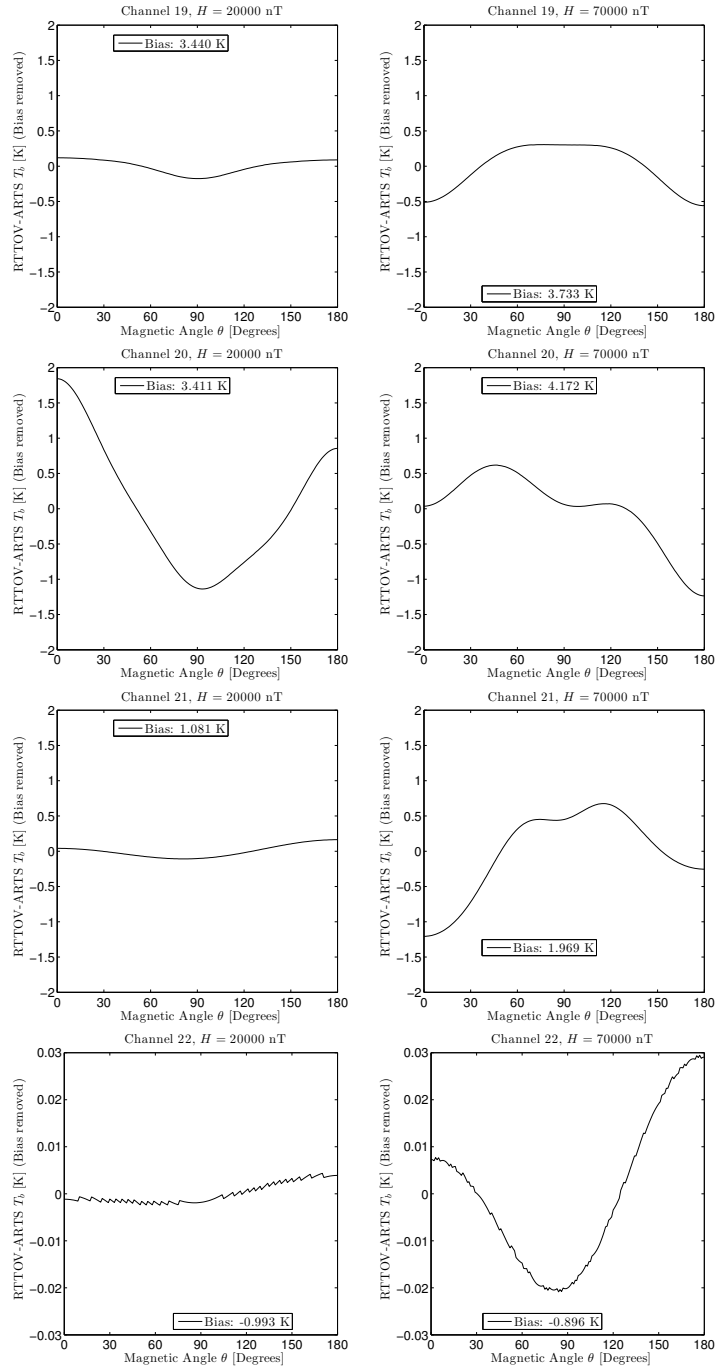
Figure 12: Angular dependency in bias of RTTOV to ARTS. The plot titles indicate which channel and the strength of the magnetic field. Each plot has removed the average bias. Both models are run for the mean profile of Figure 1 at an viewing angle consistent with SSMIS (55° at the surface).
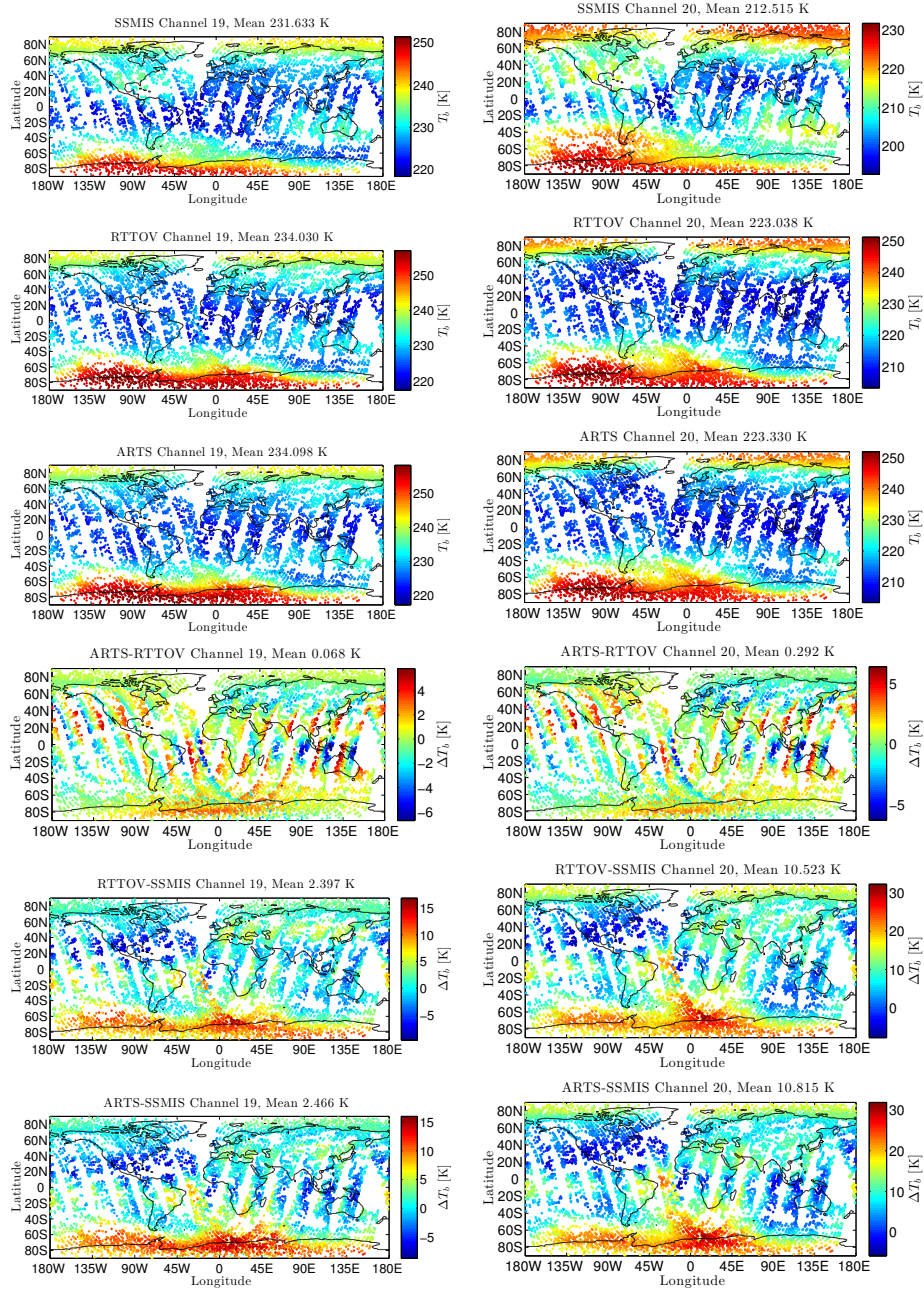
Figure 13: Channel 19 and 20 global comparison between ARTS and RT-TOV and SSMIS raw data. The data is from 2013-09-25. To the left is channel 19 and to the right is channel 20. The content of this figure is explained in the text.
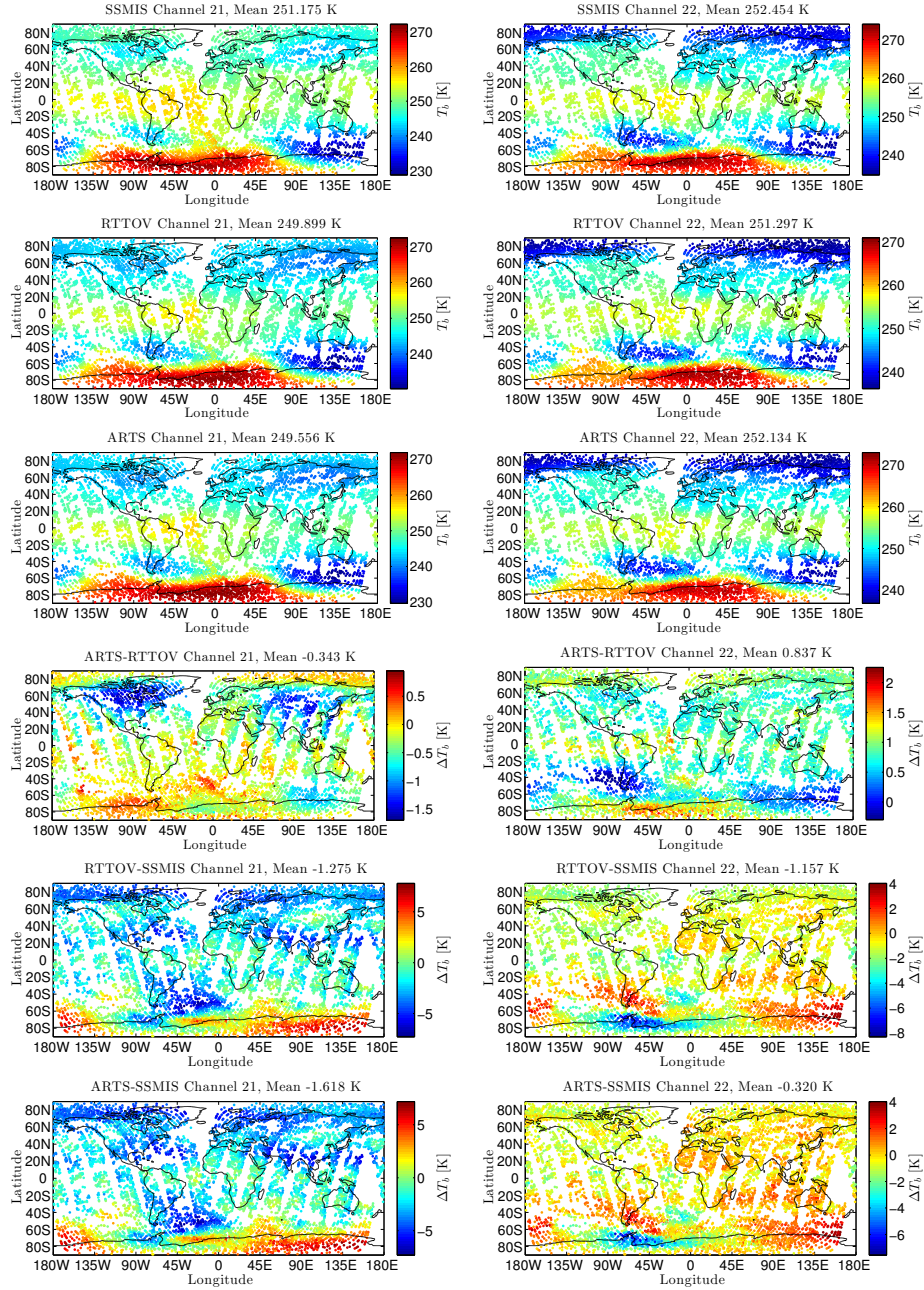
Figure 14: Channel 21 and 22 global comparison between ARTS and RT-TOV and SSMIS raw data. The data is from 2013-09-25. To the left is channel 21 and to the right is channel 22. The content of this figure is explained in the text.
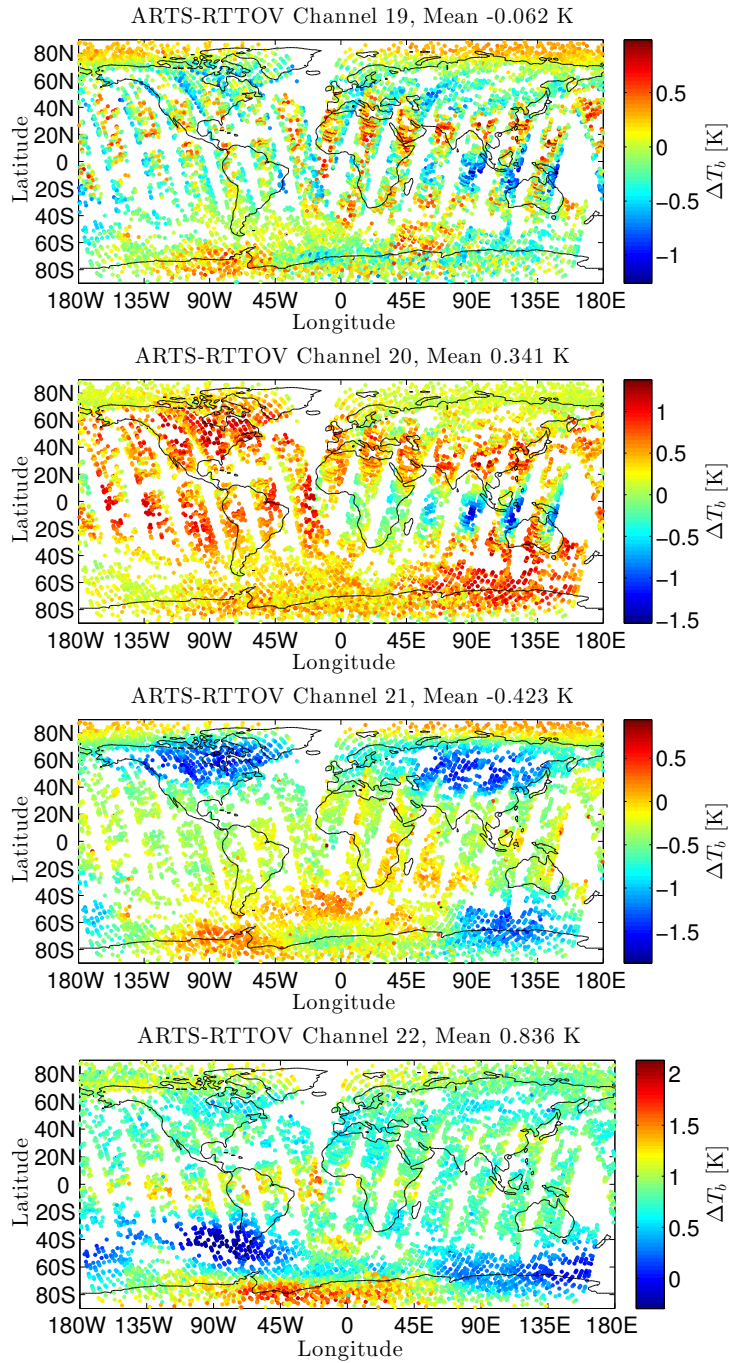
Figure 15: All channel global comparison between ARTS and RTTOV for SSMIS NWP atmospheres. The data is from 2013-09-25. The plot titles indicates SSMIS channel. These plots the same as the model comparisons of Figure 13 and 14, but the magnetic field has been kept constant for ARTS simulations.